L.O. Copy

L.O. NAE-503 FILE BM2-17-14A-31 PREPARED BY L.T. Conlin CHECKED BY J.L.	NATIONAL AERONAUTICAL ESTABLISHMENT OTTAWA, CANADA LABORATORY MEMORANDUM SECTION Aerodynamics	NO. AE-46N PAGE 1 OF COPY NO. 14 DATE October 1957

SECURITY CLASSIFICATION ~~SECRET~~

SUBJECT Wind Tunnel Tests of 0.04 Scale Model of Avro C-105 Vertical Tail at Supersonic Speeds

PREPARED BY L.T. Conlin

ISSUED TO
Dr. D.C. MacPhail
Mr. J.H. Parkin
✓ Mr. R.J. Templin (2)
Mr. J. Lukasiewicz (2)
Author
Aero Library (2)

Introduction

Tests have been made in the N.A.E. 30" x 16" high speed wind tunnel on a 0.04 scale model of the vertical tail of the C-105 aircraft to determine the vertical tail load characteristics and rudder hinge moment data. The tests were made at Mach numbers 1.22, 1.35, 1.57, 1.78 and 2.03. The corresponding Reynolds number range is shown in figure 4.

Test Model

The model consisted of the vertical tail and filler block from the 0.04 scale Cornell Aeronautical Laboratories Model of the C-105 aircraft. It was mounted on a circular adaptor plate for installation in the NAE wind tunnel. The adaptor plate was arranged so that it could be rotated in its mounting and clamped at the various settings corresponding to the required values of angle β.

The model was equipped with a 3-component strain gauge balance (side force, root bending moment and yawing moment) and each of the six interchangeable rudders was equipped with strain gauges to measure rudder hinge moment.

Photographs of the model appear in figure 1 and a drawing in figure 2.

Balance Calibration

The three-component balance and the rudder hinge moment balances were calibrated prior to the tests over the range of loadings anticipated. A check calibration was made on completion of the test programme. This indicated no change from the original calibration, although it was apparent that in the case of the rudders, variation

in contact resistance at the connector could cause considerable error. In such case, however, it was found that on cleaning the contacts carefully and reassembling, the original calibration checked satisfactorily.

Deflections of the fin and rudder under load were also measured.

Test Conditions

The tests were made at Mach numbers 1.22, 1.35, 1.57, 1.78 and 2.03. For angle β equal to zero, tests were made at each Mach number with rudder angle (δ_r) -5, +5, 10, 20, 30 (nominal values). With δ_r equal to zero, tests were made at each Mach number for the following values of angle β : -4, -2, -1, 0, 1, 2, 4, 6, 8, 10, and 12 degrees.

Reynolds number, based on the fin mean geometric chord, was approximately 2.3×10^6 at the lower Mach numbers and about 1.96×10^6 at Mach number 2.03, see fig. 4.

Interference Effects

Interference due to blockage and possibly shock wave reflection was encountered at Mach number 1.22, at the higher values of β (10° and 12°).

Also, since it was impossible to use a boundary layer shim as is customary in half-model tests in the 30" x 16" wind tunnel, the portion of the fin close to the wall lay in the boundary layer.

No correction for these effects have been applied, and the results for M 1.22 at β equal to 10° and 12° have been ignored.

Coefficients and Symbols

The measurements of vertical tail load are referred to an axis system parallel to the body axis system. This is illustrated in

figure 3.

Coefficients and symbols are defined as follows:

C_{Y_v} side force coefficient of vertical tail, $\frac{Y_v}{q S_v}$

C_{B_v} root bending-moment coefficient of vertical tail about the theoretical vertical tail root (1.28 inch above fuselage reference line), $\frac{B_v}{q S_v b_v}$

C_{n_v} yawing moment coefficient of vertical tail about a vertical axis through the 25 per cent point of the vertical tail mean geometric chord, $\frac{n_v}{q S_v \bar{c}_v}$

C_{h_r} rudder hinge moment coefficient, $\frac{H_r}{q S_r \bar{c}_r}$

$$\frac{x_{a.c.}}{\bar{c}_v} = 0.25 - \left(\frac{\partial C_{n_v}}{\partial C_{Y_v}}\right)_{\delta_r = 0^\circ}$$

$$\frac{x_{c.p}}{\bar{c}_v} = 0.25 - \frac{\left(\partial C_{n_v}/\partial \delta_r\right)_{\beta=0^\circ}}{\left(\partial C_{Y_v}/\partial \delta_r\right)_{\beta=0^\circ}}$$

$$\frac{y_{c.p}}{b_v} = \frac{\left(\partial C_{B_v}/\partial \delta_r\right)_{\beta=0^\circ}}{\left(\partial C_{Y_v}/\partial \delta_r\right)_{\beta=0^\circ}}$$

a_1 rate of change of side force coefficient with angle of sideslip, β

a_2 rate of change of side force coefficient with rudder angle, δ_r

C_{h_β} rate of change of hinge moment coefficient with angle of sideslip, β

$C_{h_{\delta_r}}$ rate of change of hinge moment coefficient with rudder angle, δ_r

q free stream dynamic pressure

S_v vertical tail area (from the theoretical root chord), 36.586 square inches.

S_r rudder area (aft of hinge) 8.949 square inches

$\bar{c}_v$ mean geometric chord of vertical tail, 6.497 inches

$\bar{c}_r$ rudder r m s chord, 1.911 inch

b_v span of vertical tail (from theoretical root) 6.180 in.

β angle of sideslip, degrees

δ_r rudder deflection, degrees, measured perpendicular to hinge line

x_{ac} distance of aerodynamic center from the leading edge of $\bar{c}_v$

x_{cp} distance of the centre of pressure from the leading edge of $\bar{c}_v$ due to rudder deflection

y_{cp} distance of the centre of pressure from the vertical tail root chord, due to rudder deflection

Corrections and Accuracy

Nominal and measured values of rudder angle are tabulated below in Table I for no load condition.

Table I

Rudder Angle, δ_r

Nominal	Measured
-5 degrees	-5.34 degrees
0	-0.13
5	4.90

10 degrees	9.67 degrees
20	19.55
30	29.61

The measured values of δ_r corrected for deflection under load, and the values of β corrected for deflection have been used in plotting results.

The estimated possible errors in measured quantities are as follows:

$C_{Y_v} \pm .006$

$C_{n_v} \pm .003$

$C_{B_v} \pm .0019$

$C_{l_{r_v}} \pm .0015$

Results

The results of the tests are presented in figures 5 to 20, where measured quantities are plotted as follows:

C_{Y_v}	vs	β	figure 5
C_{Y_v}	vs	δ_r	figure 6
C_{n_v}	vs	β	figure 7
C_{n_v}	vs	δ_r	figure 8
C_{n_v}	vs	C_{Y_v}	figure 9
$C_{l_{r_v}}$	vs	β	figure 10
$C_{l_{r_v}}$	vs	δ_r	figure 11
C_{B_v}	vs	β	figure 12
C_{B_v}	vs	δ_r	figure 13
a_1	vs	M	figure 14
a_2	vs	M	figure 15

a.c. fin	vs	M	figure 16
c.p. "	vs	M	figure 17
δ_{cp} "	vs	M	figure 18
C_{h_β}	vs	M	figure 19
$C_{h_{\delta_r}}$	vs	M	figure 20

View of Model

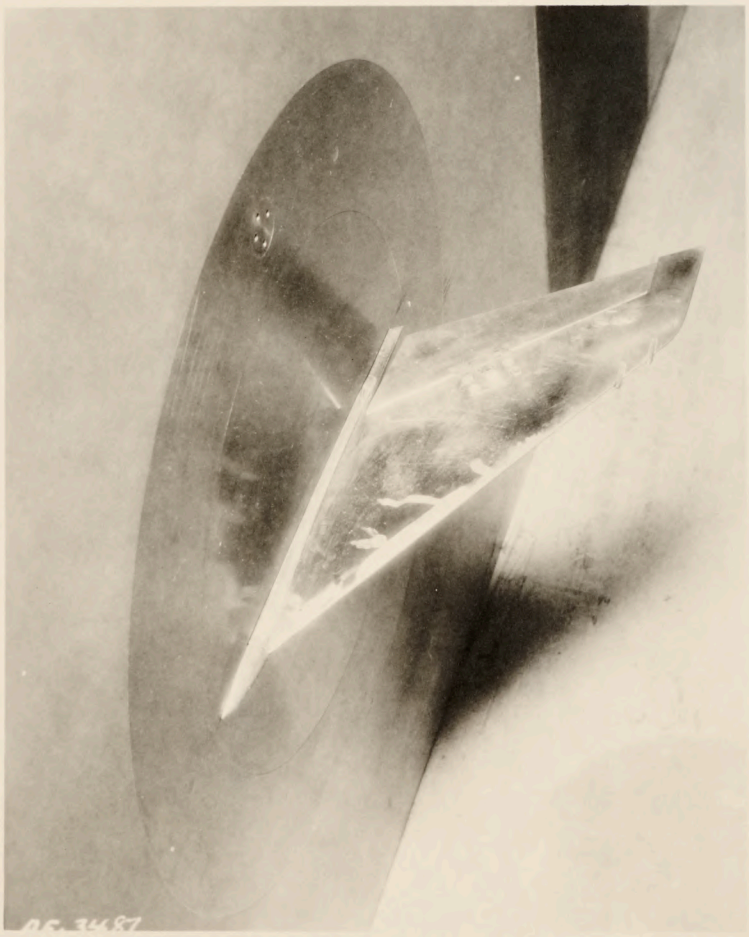

Model in NAE Tunnel

Fig. 1 The .04 Scale AVRO C-105 Vertical Tail

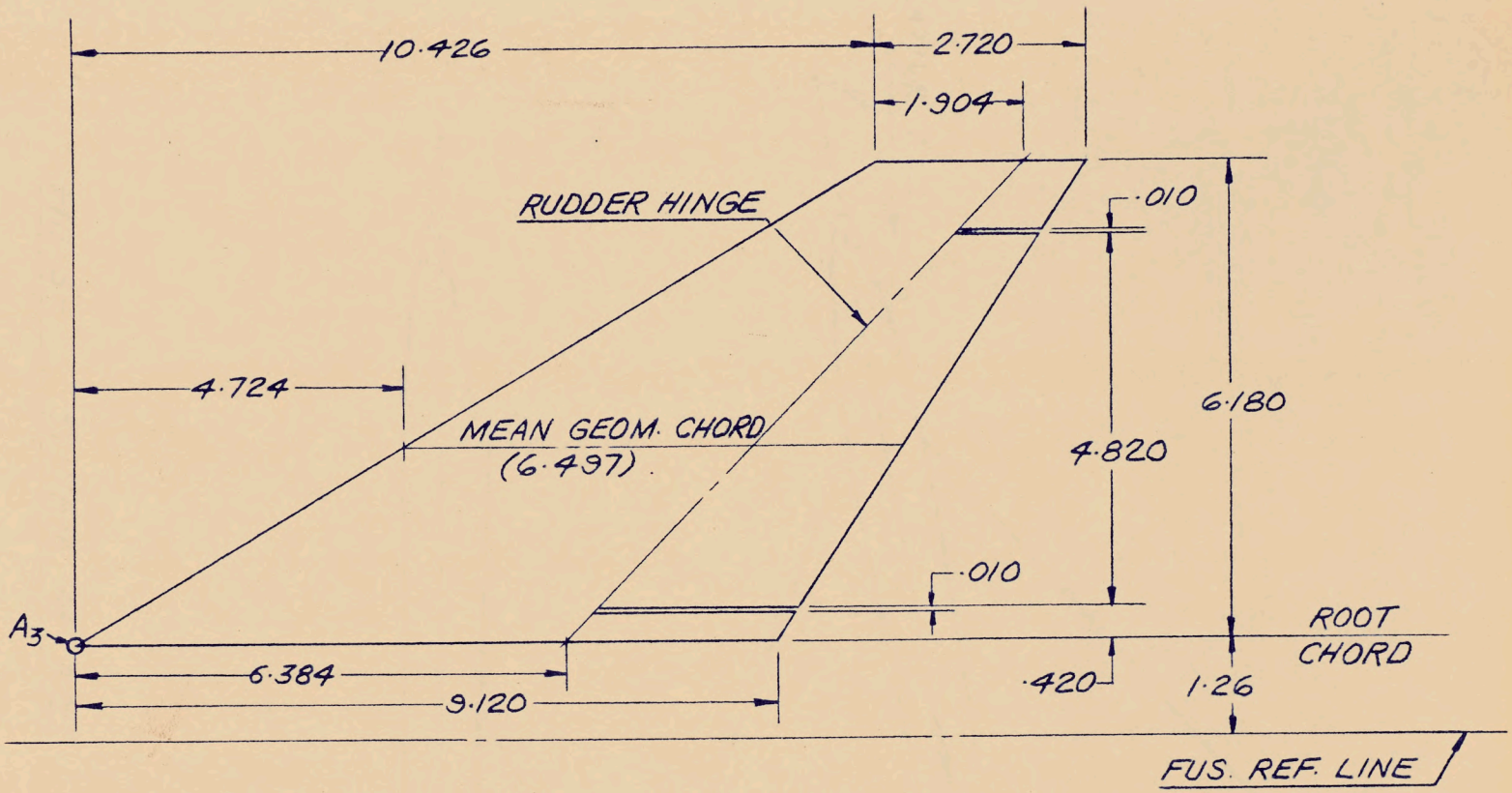

FIG. 2— C-105 VERTICAL TAIL, ·04 SCALE

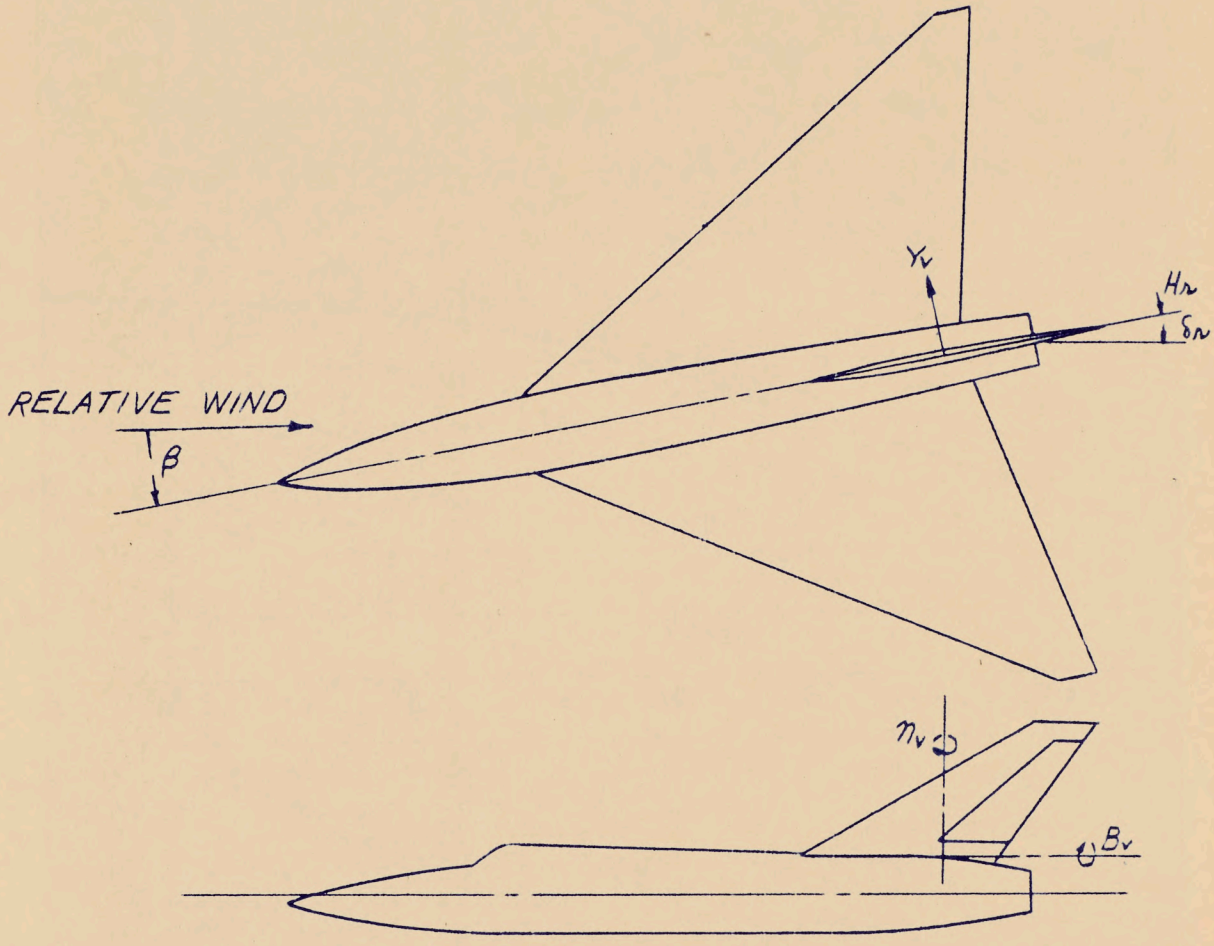

FIG. 3- SYSTEM OF AXES

FIG. 4

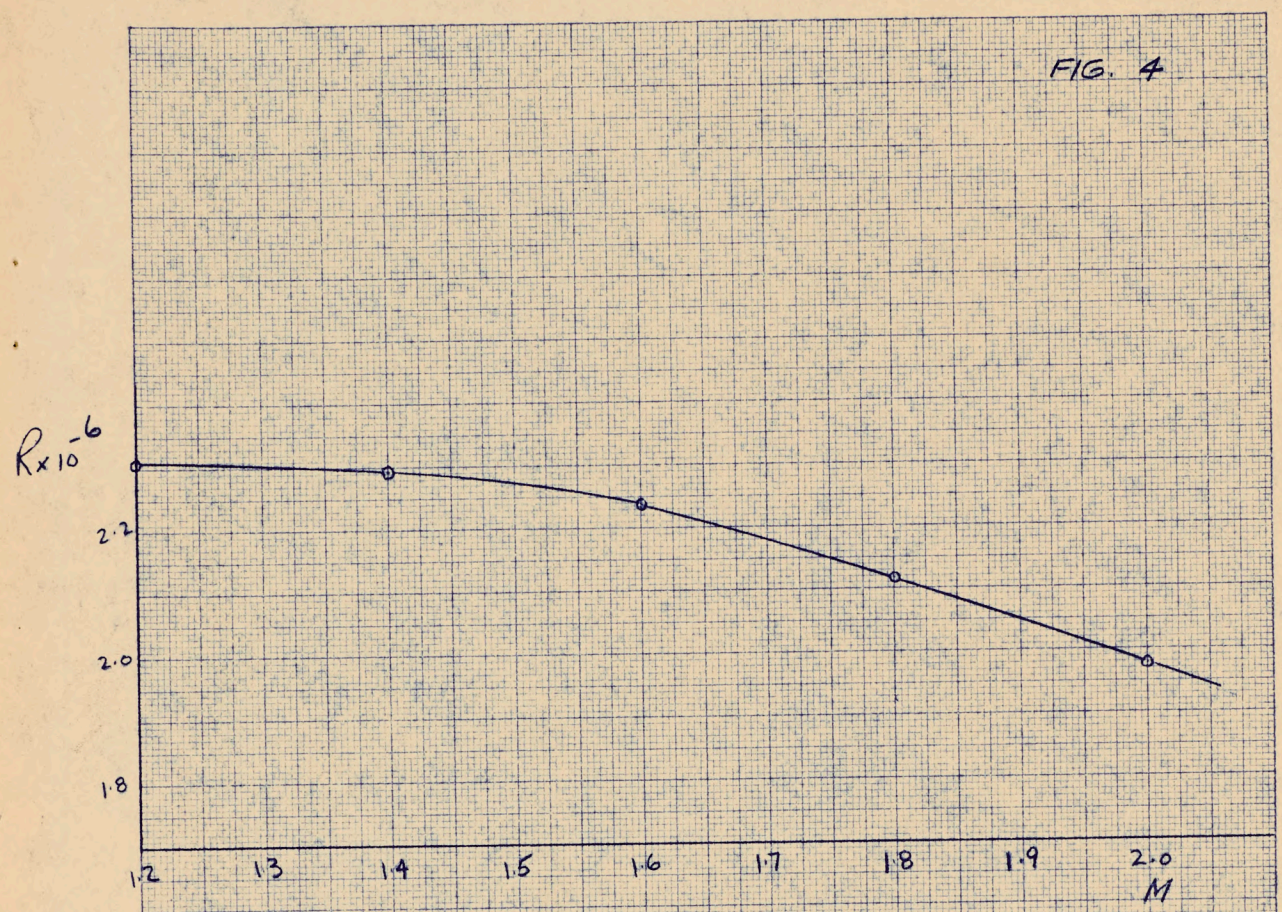

MODEL REYNOLDS NUMBER (BASED ON FIN MEAN GEOMETRIC CHORD) VERSUS MACH NUMBER

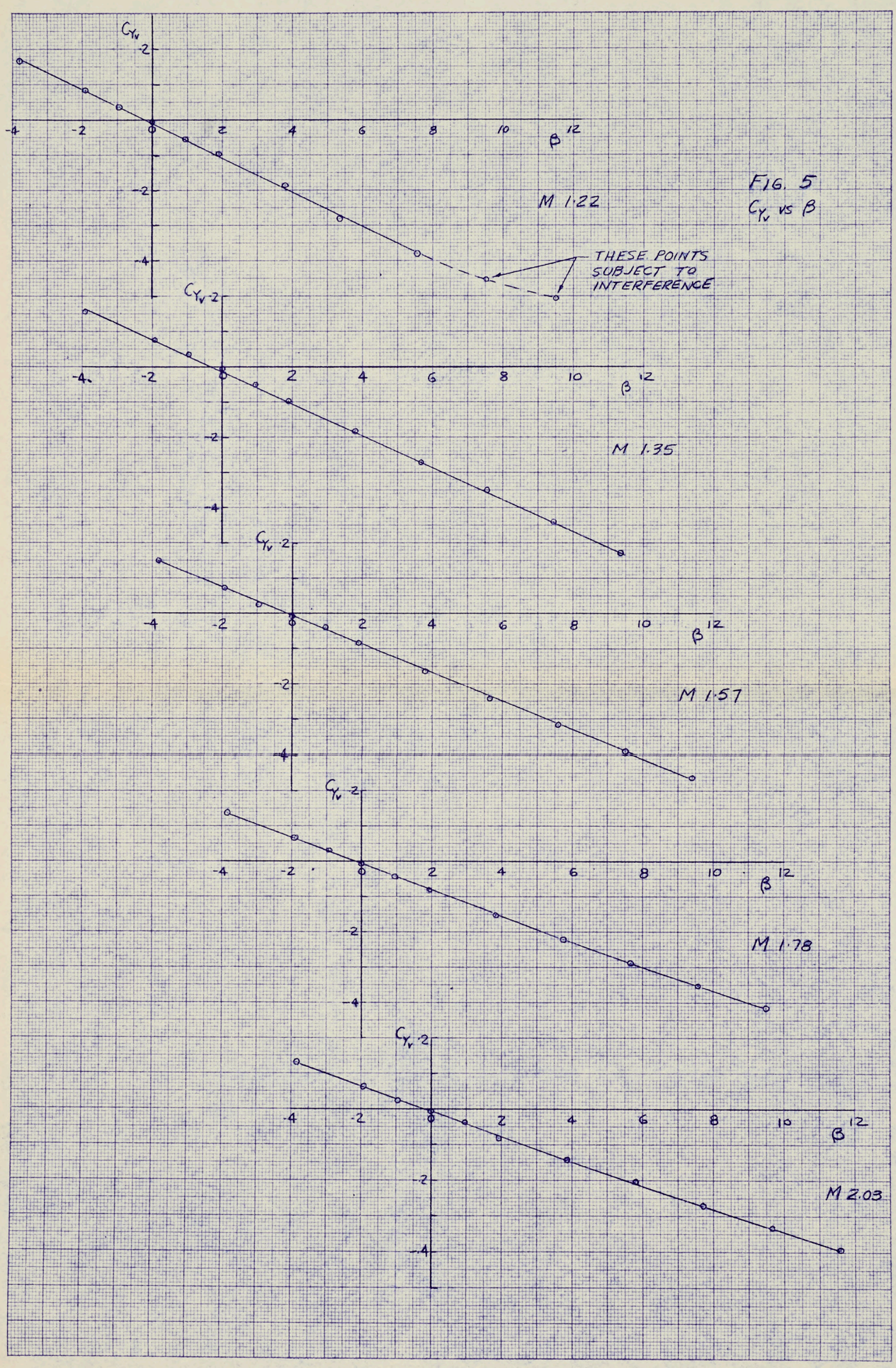
C_{Y_v}
β
M 1.22
THESE POINTS SUBJECT TO INTERFERENCE
M 1.35
M 1.57
M 1.78
M 2.03

FIG. 5
C_{Y_v} vs β

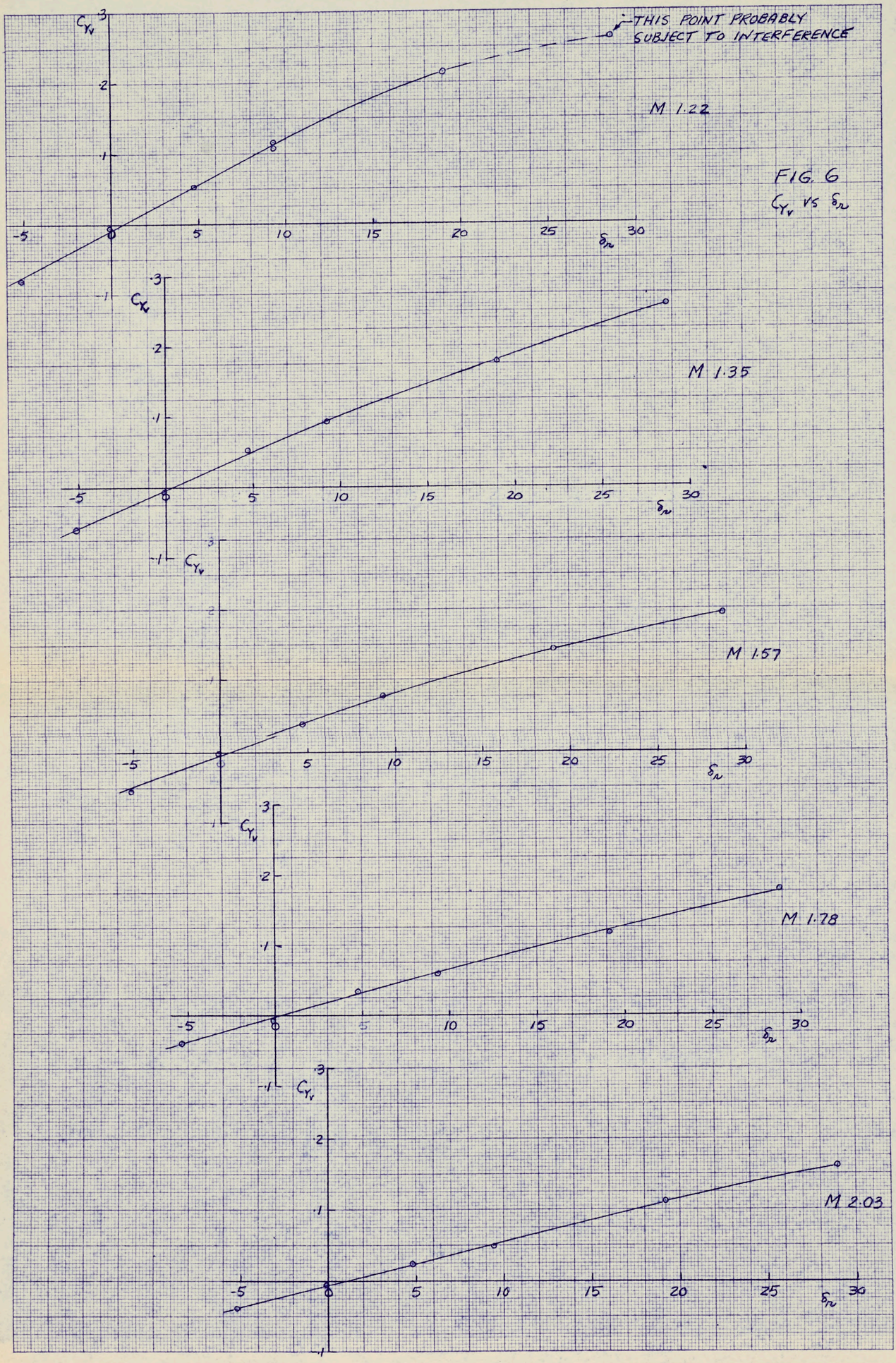

FIG. 6
C_{Y_v} vs δ_R

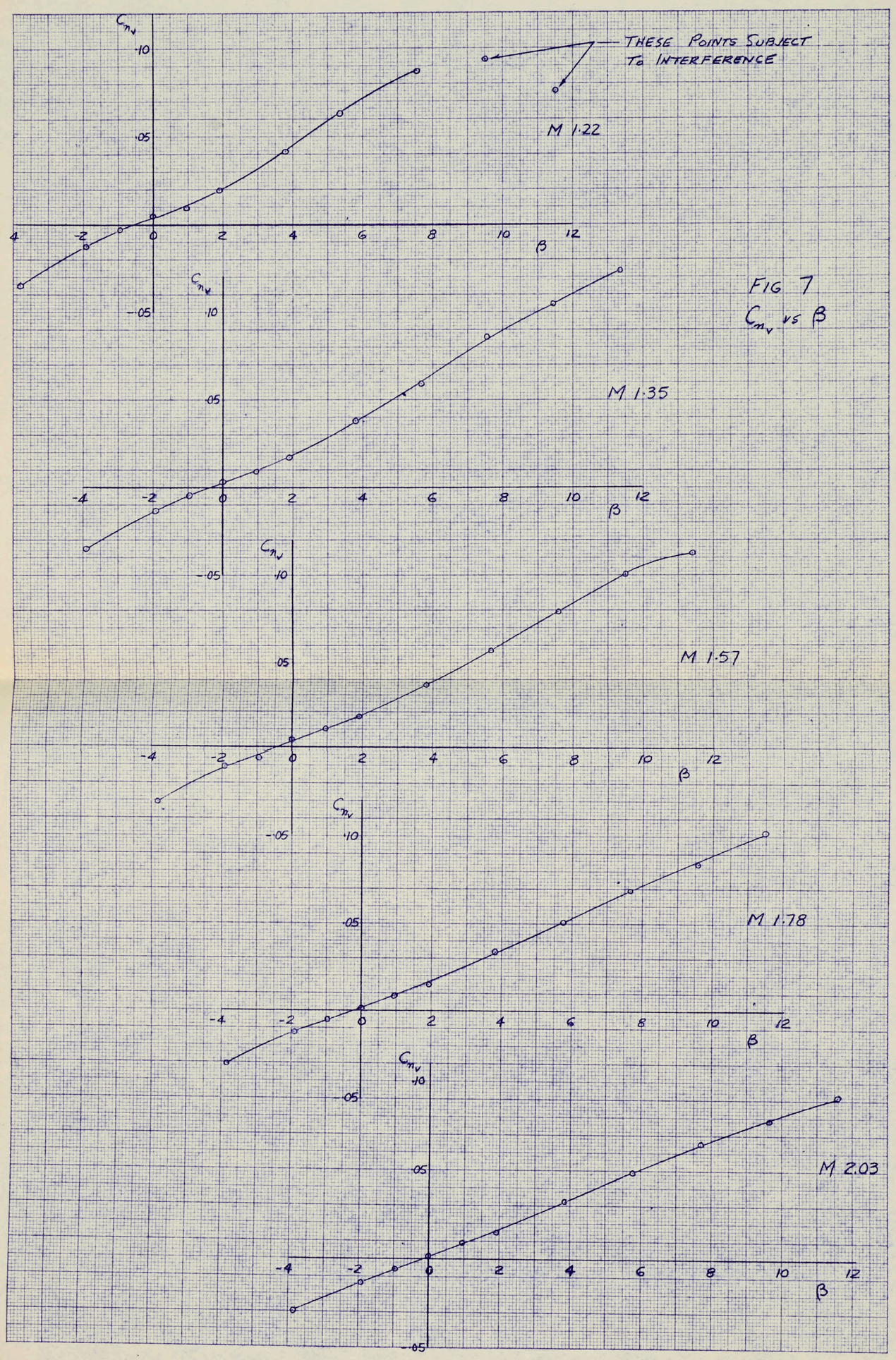
C_{m_v}
.10
.05
-.05
-4
-2
0
2
4
6
8
10
12
β
THESE POINTS SUBJECT TO INTERFERENCE
M 1.22
M 1.35
M 1.57
M 1.78
M 2.03

FIG 7
C_{m_v} vs β

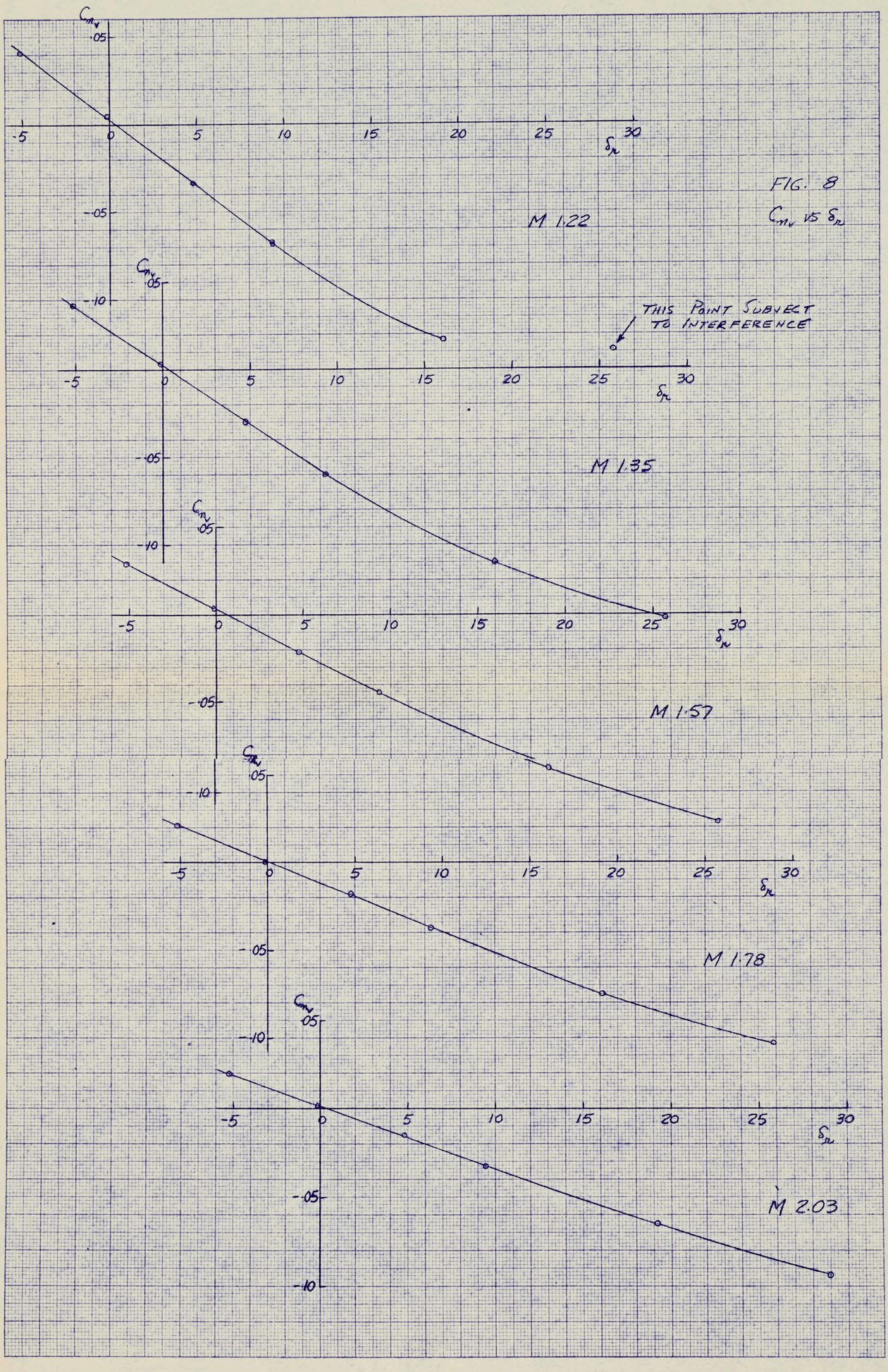

FIG. 8
C_{m_v} vs δ_R

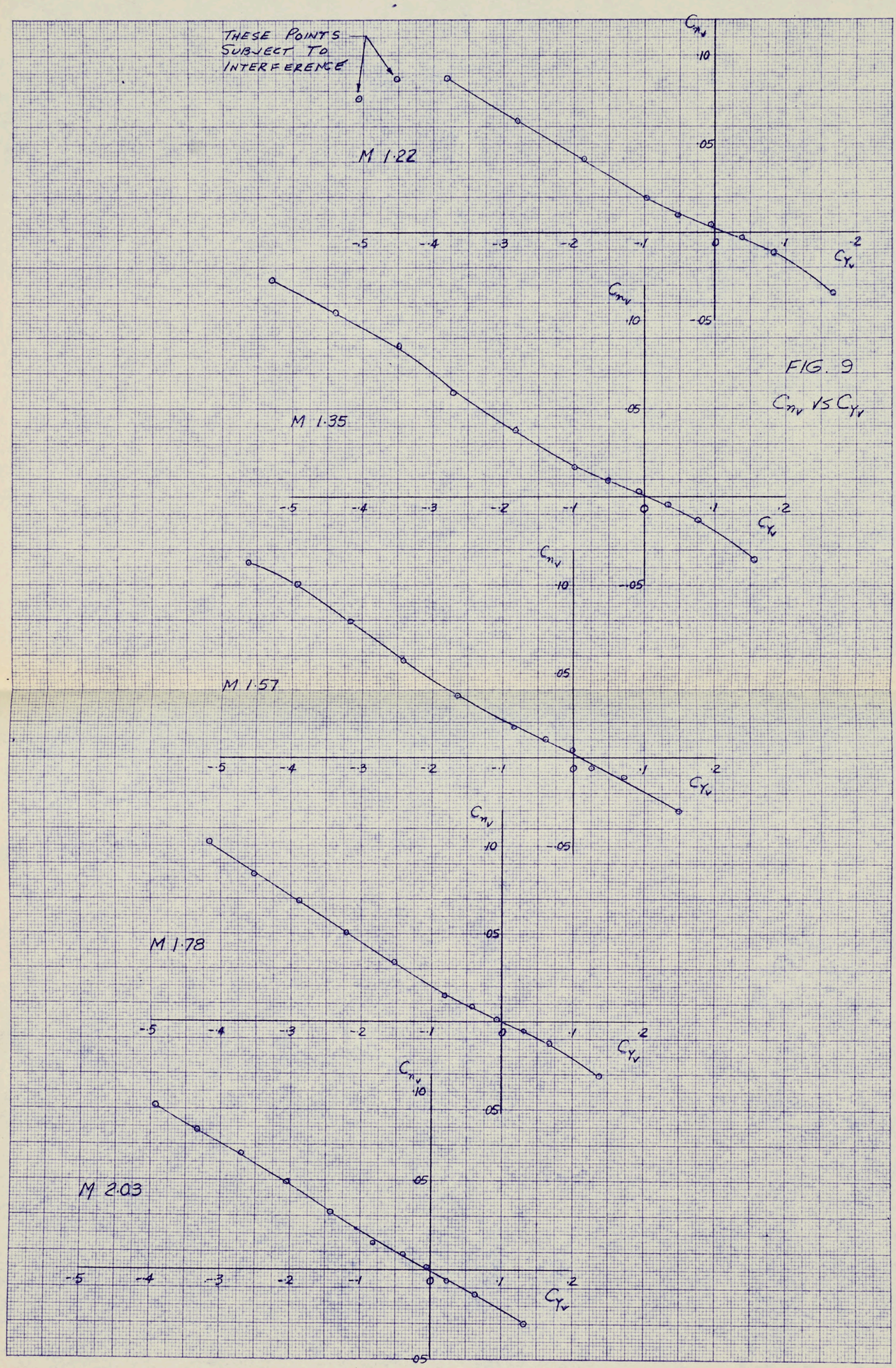

FIG. 9

C_{m_v} VS C_{Y_v}

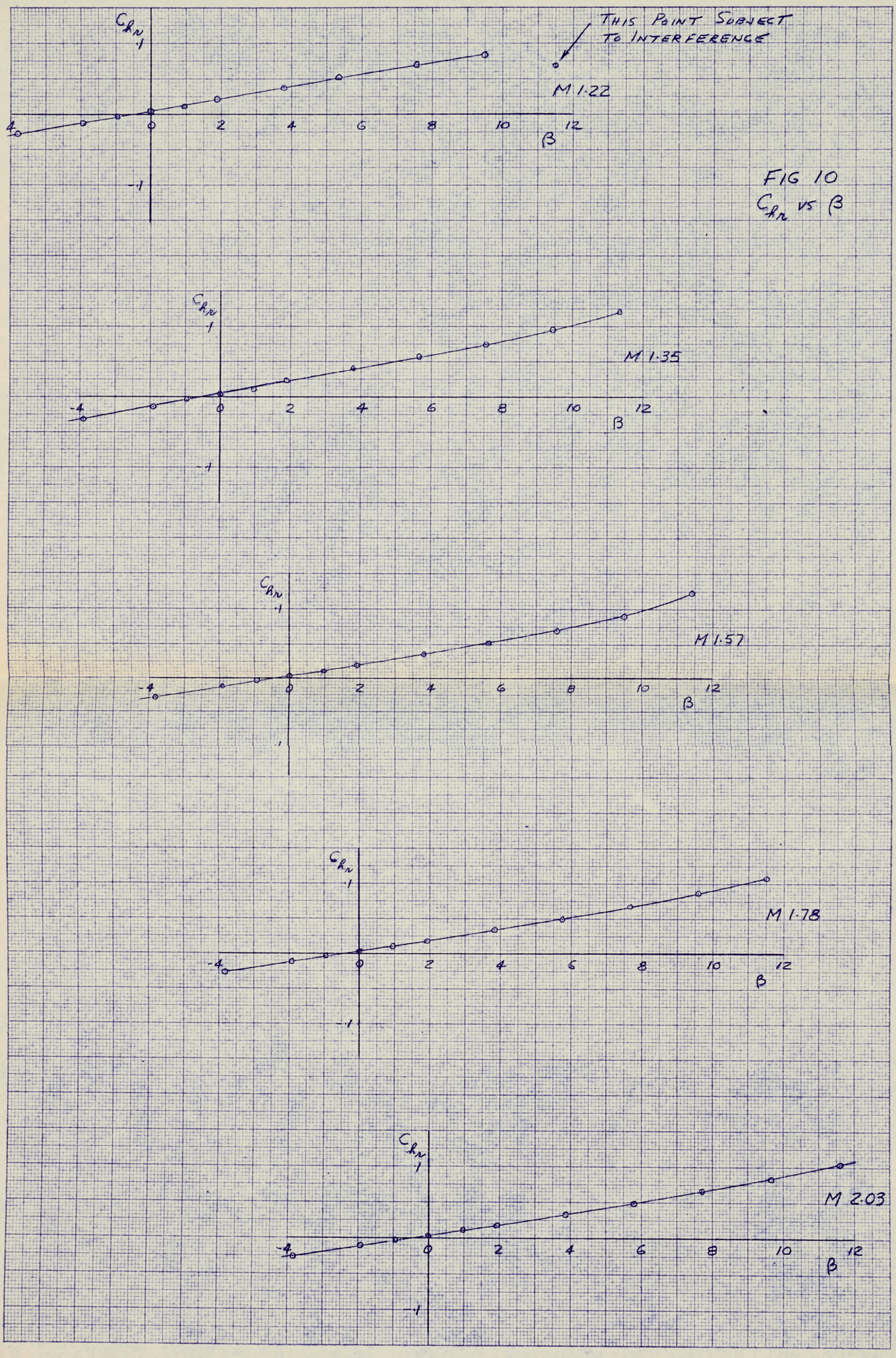

FIG 10
C_{l_N} vs β

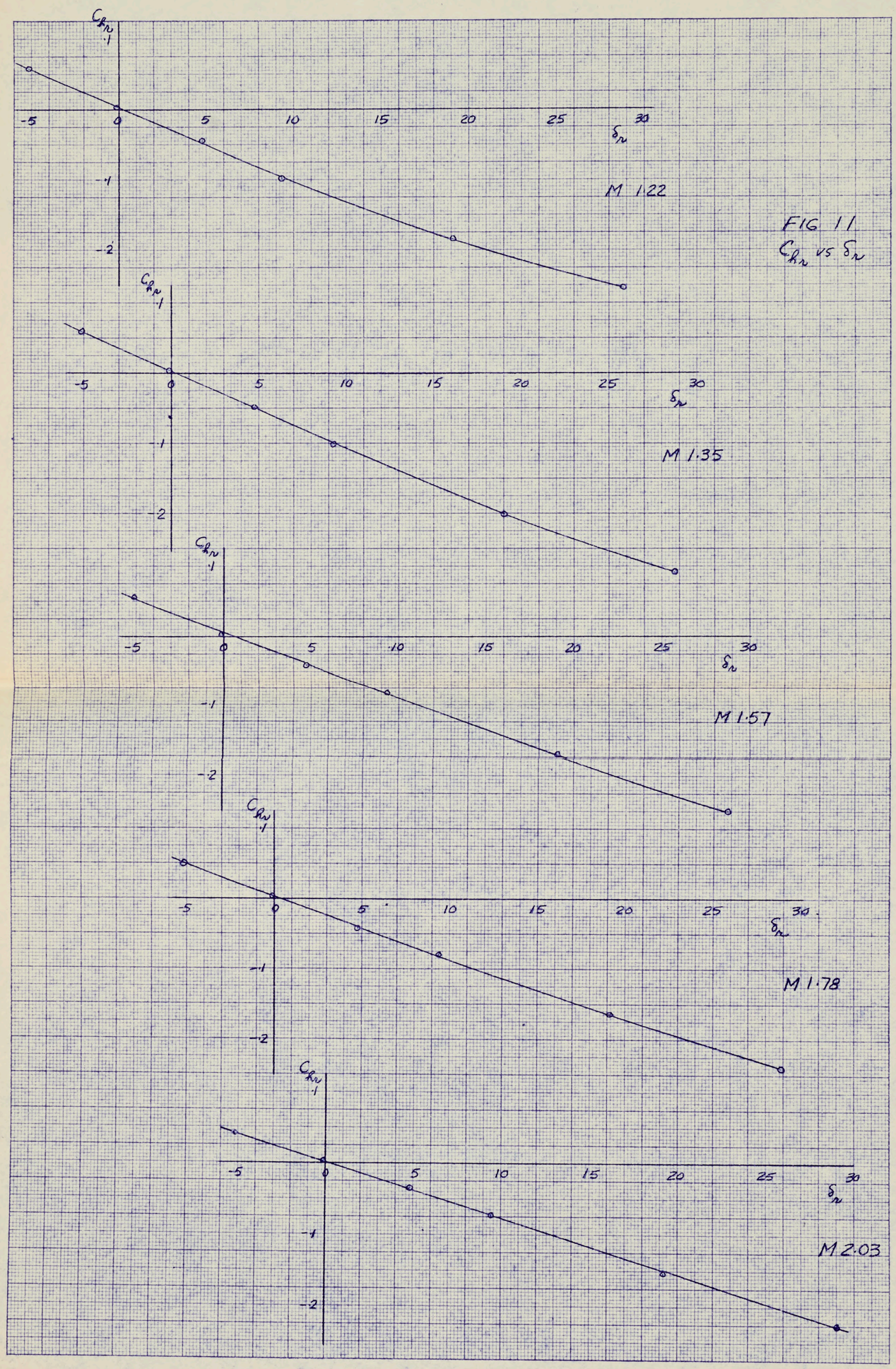

FIG 11
C_{h_N} vs δ_N

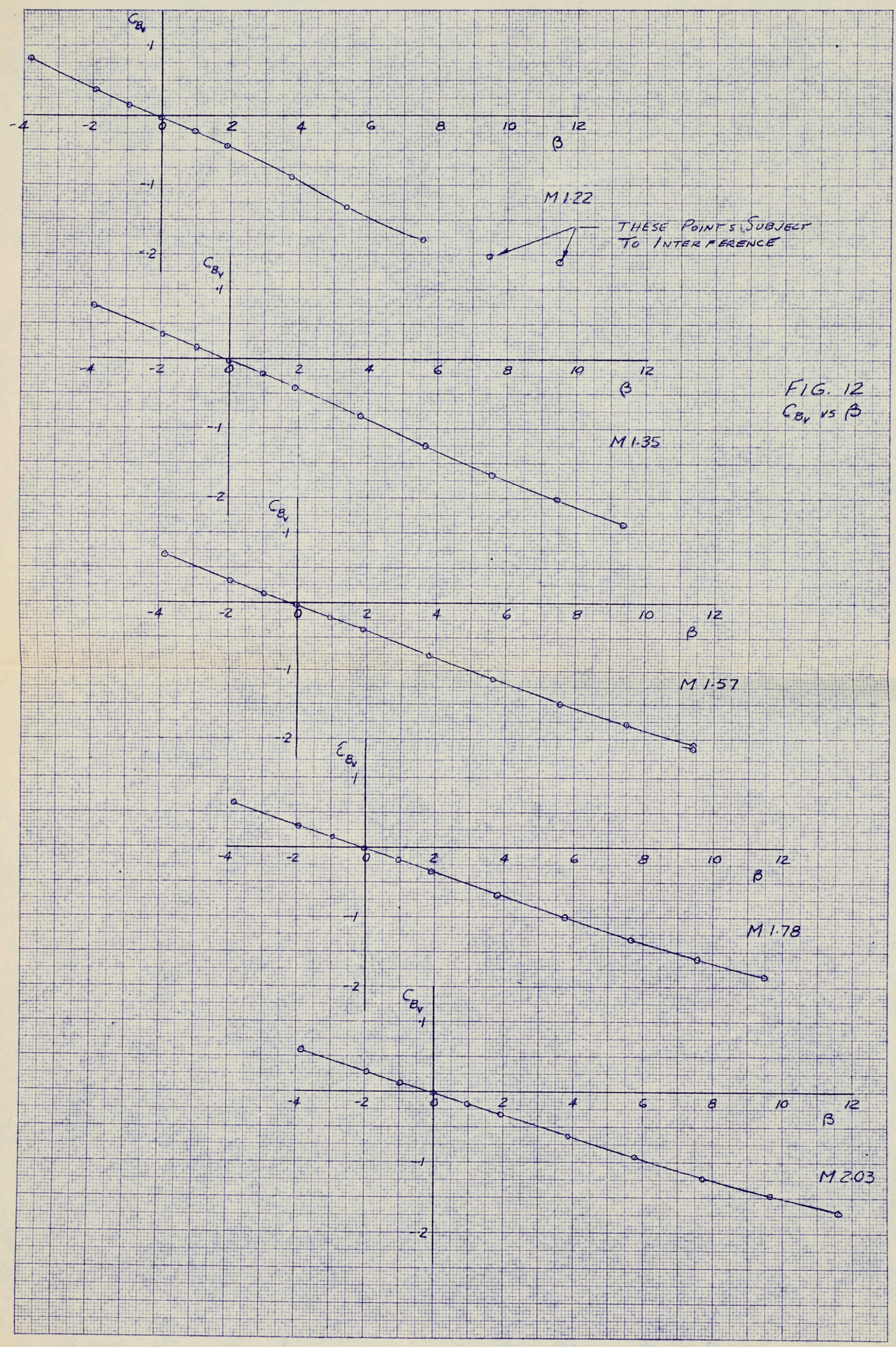

FIG. 12
C_{B_V} vs β

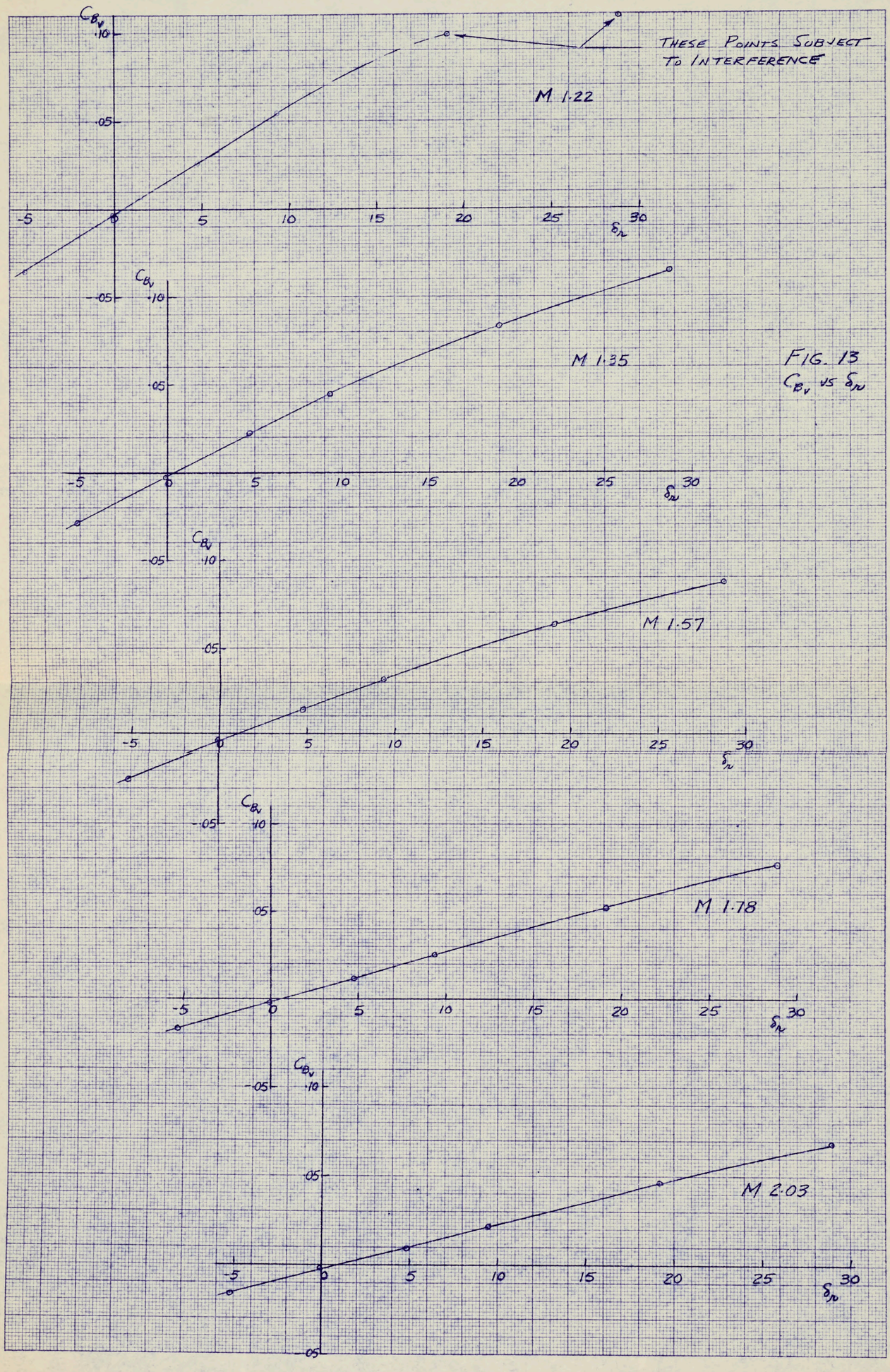

FIG. 13
C_{B_V} vs δ_N

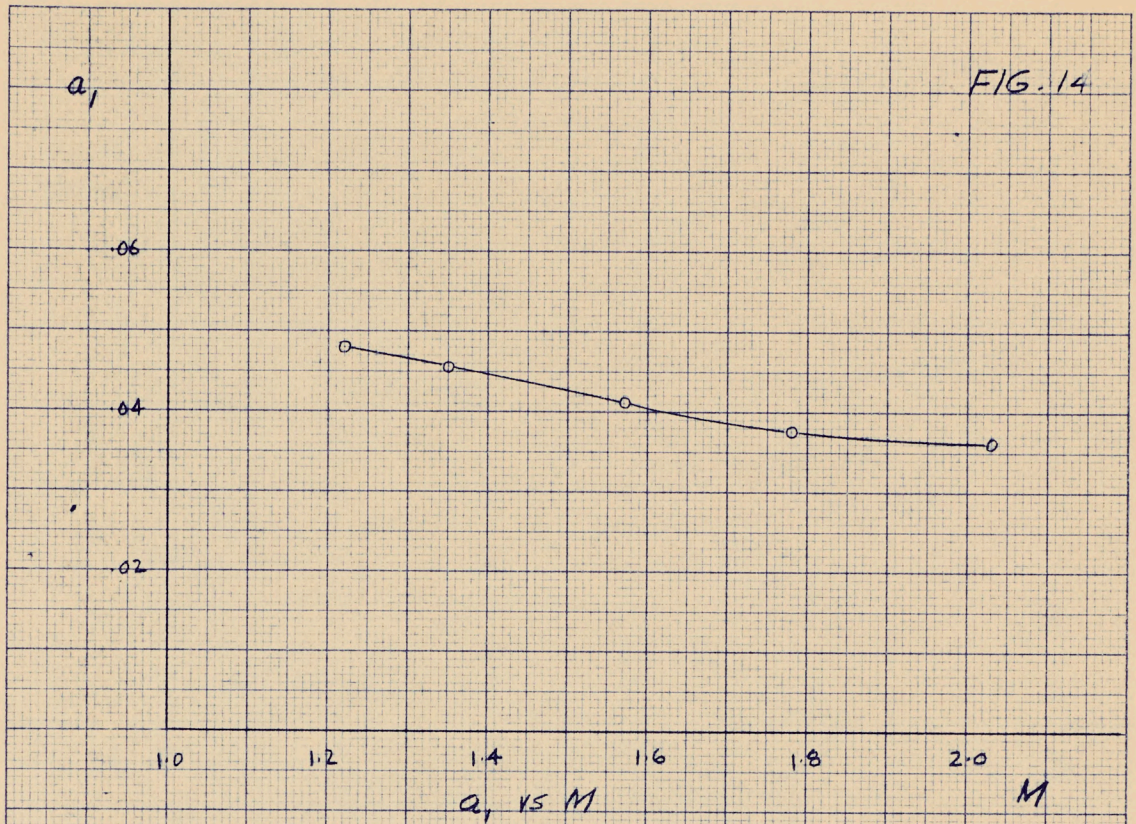

FIG. 14

a_1 vs M

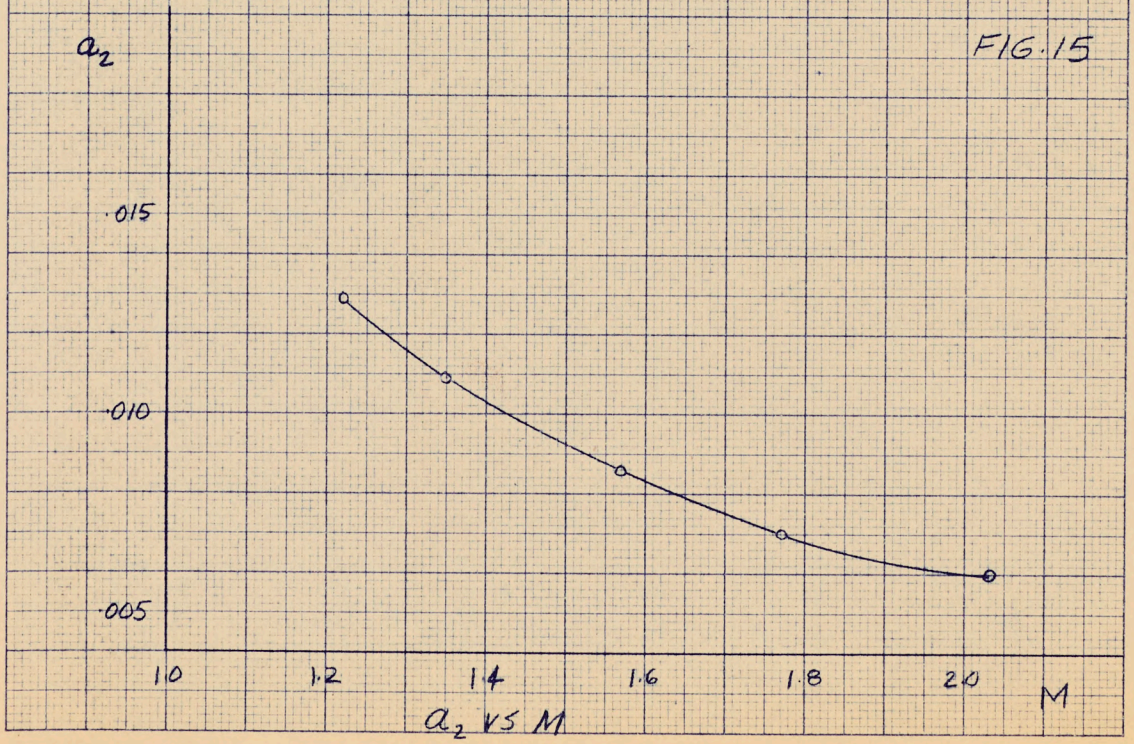

FIG. 15

a_2 vs M

FIG. 16

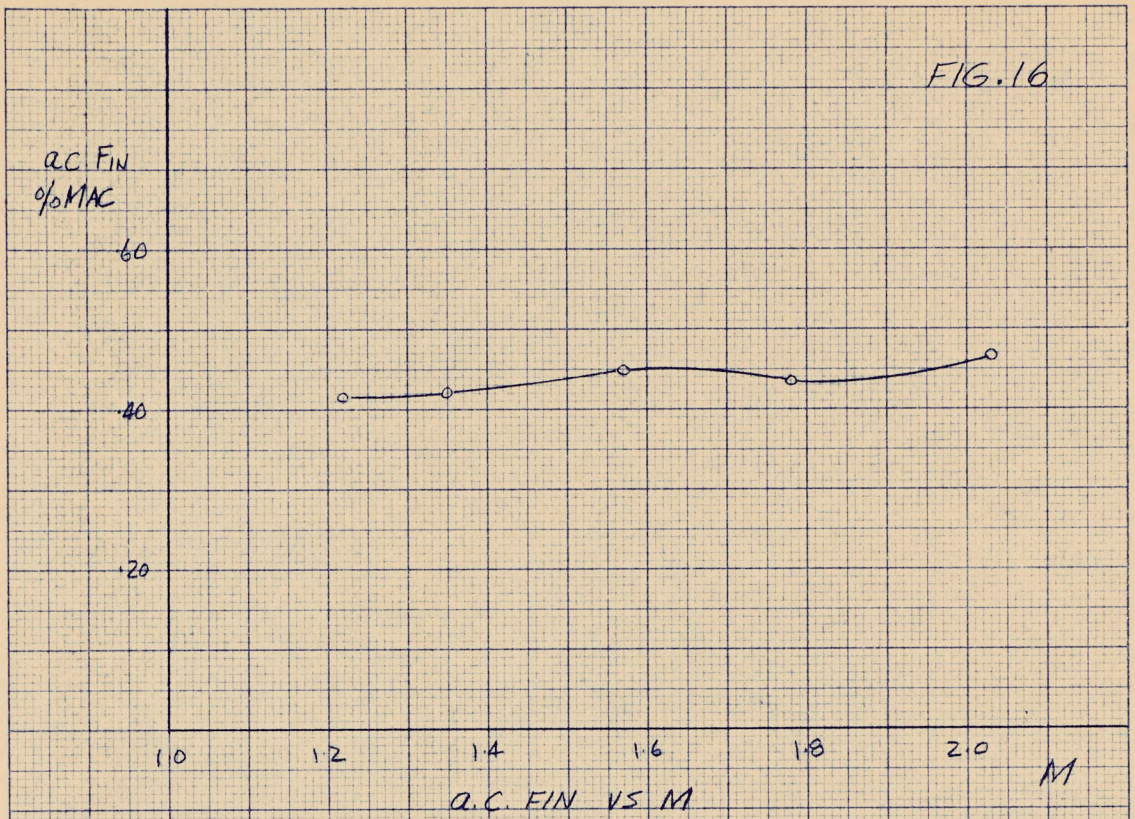

a.c. FIN VS M

FIG. 17

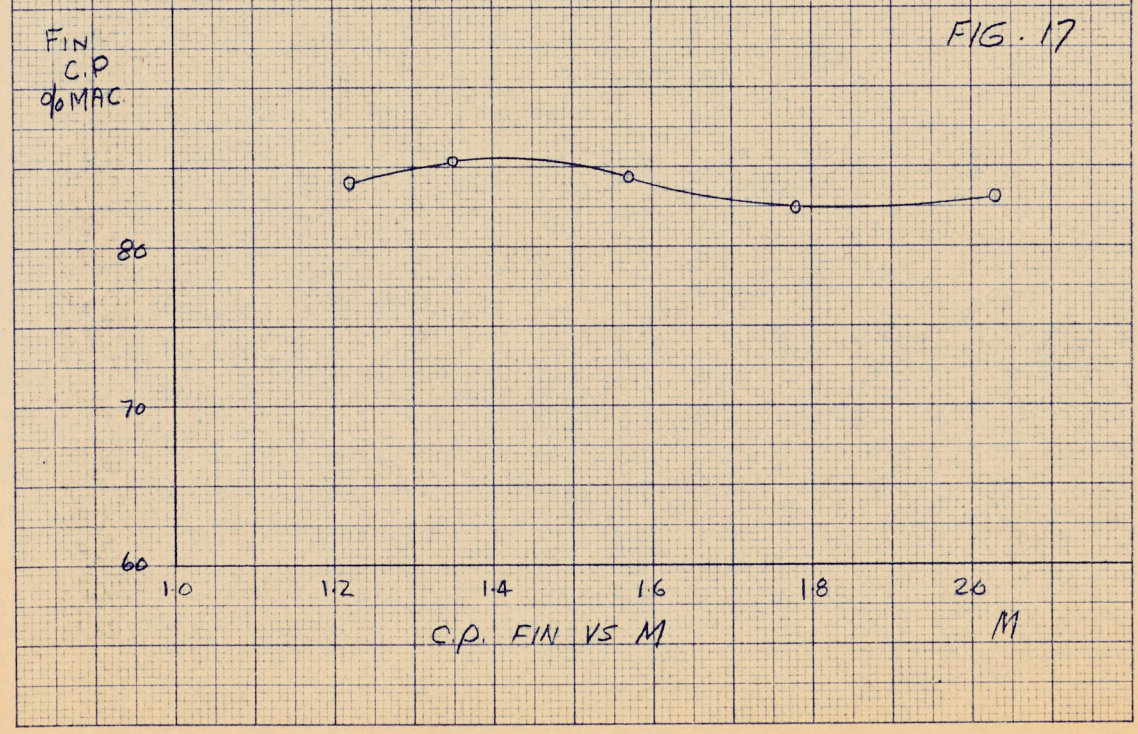

C.P. FIN VS M

FIG. 19

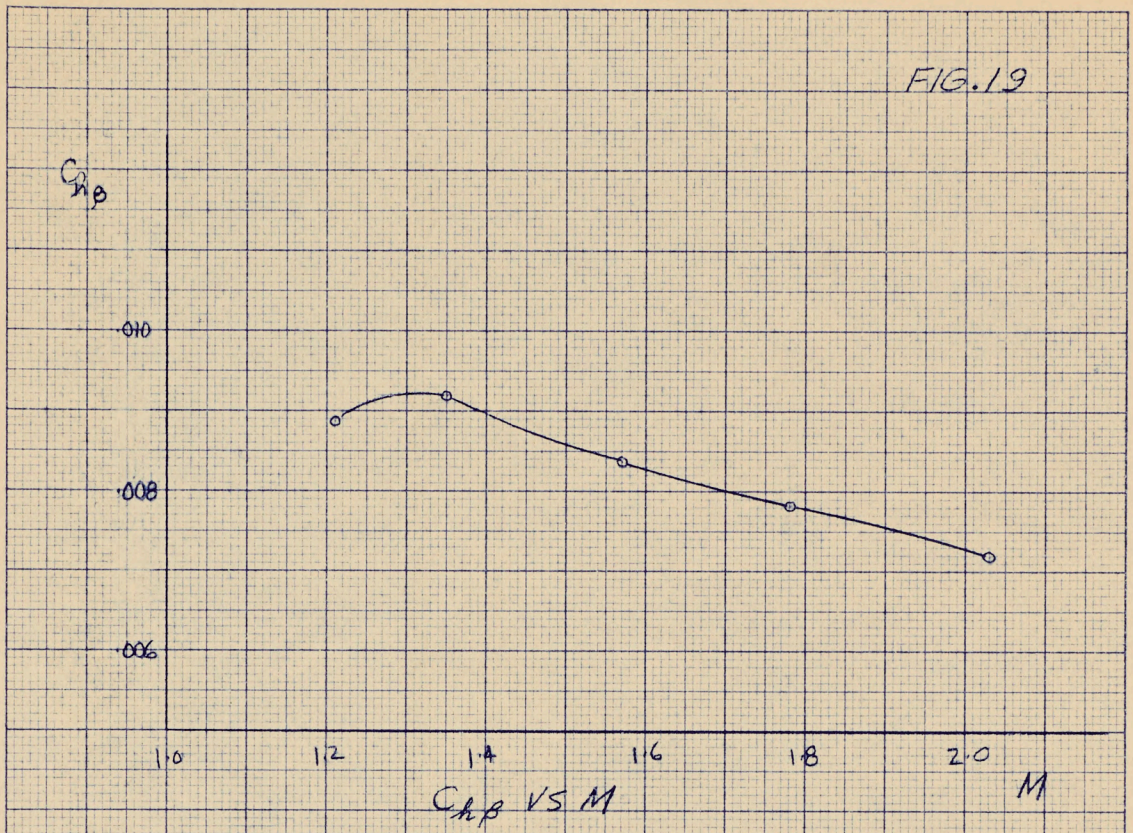

C_{h_β} VS M

FIG. 20

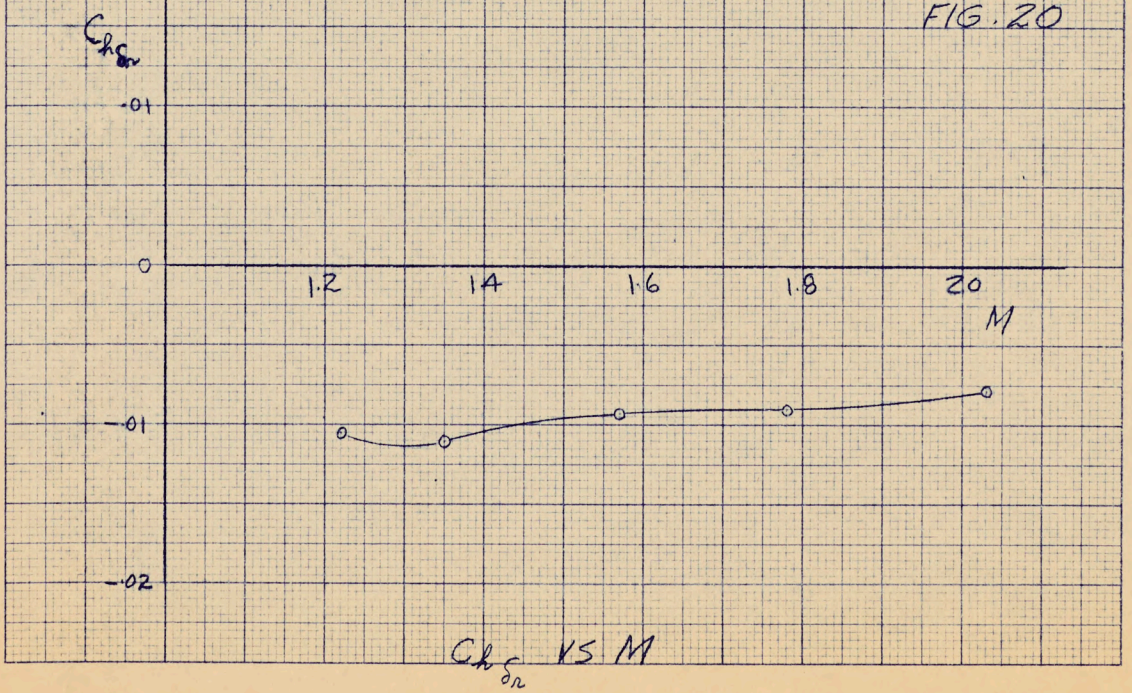

$C_{h_{\delta_R}}$ VS M